Loss Compensation and Superresolution in Metamaterials with Excitations at Complex Frequencies

Seunghwi Kim[1,†], Yu-Gui Peng,[1,2,†] Simon Yves,[1] and Andrea Alù[1,3,*]

[1]*Photonics Initiative, Advanced Science Research Center,*
City University of New York, New York, New York 10031, USA
[2]*School of Physics, Huazhong University of Science and Technology, 430074 Wuhan, China*
[3]*Physics Program, Graduate Center, City University of New York, New York, New York 10016, USA*

Metamaterials, from optics to radio frequencies and acoustics, have attracted significant attention over the last few decades, with promising applications in a wide range of technological areas. However, it has been recognized that their performance is often hindered by ubiquitous material loss and nonlocal phenomena. A canonical problem consists in imaging through metamaterial superlenses, which hold the promise of superresolution but which are, in practice, limited by material loss as we attempt to image deeply subwavelength details. Active metamaterials have been explored to compensate for loss; however, material gain introduces other obstacles, e.g., instabilities, nonlinearity, and noise. Here, we demonstrate that the temporal excitation of passive metamaterials using signals oscillating at complex frequencies can effectively compensate material loss, leading to resolution enhancement when applied to metamaterial superlenses. More broadly, our results demonstrate that virtual gain stemming from tailored forms of excitation can tackle the impact of loss in metamaterials, opening promising avenues for a broad range of applications from acoustic to photonic technologies.

I. INTRODUCTION

The excitement around metamaterials has been fueled by the discovery that their exotic properties may, in principle, overcome physical limits in various technological fields. Nonetheless, the inherent presence of loss in metamaterials—stemming from material absorption and scattering losses due to inhomogeneities, defects, dislocations, and surface roughness—fundamentally limits their operation and functionality [1–3]. Several approaches have been explored to mitigate these issues, including exploring new geometries that avoid strong field concentration and the use of low-loss materials [4–7]. However, these approaches have had limited success in pushing the boundaries of metamaterial applications and typically impose various trade-offs. As another effective route, metamaterials incorporating gain elements have been put forward as a potential solution for compensating material loss [8–13]. However, gain is scarce and difficult to control,

and in some instances, introducing gain may impact the optical properties of the underlying media [14,15]. In addition, adding gain may introduce instabilities, noise, and parasitic nonlinearities, and potentially lead to saturation, all of which create further challenges [16–18].

Recently, virtual gain, associated with precisely tailored transient excitations oscillating at complex frequencies, has shown an interesting potential to compensate for the detrimental effect of ubiquitous material loss without requiring gain media. In this context, we have recently shown that it is possible to overcome the limitations of passive scatterers by exciting them with complex frequency signals [19,20]. By analytically continuing the response function of a linear system, it is possible to access singularities in the complex frequency plane, which can be engaged with signals oscillating periodically with frequency $\text{Re}[\omega]$ while their amplitude is modulated by a growing or decaying exponential factor $\text{Im}[\omega]$. Provided that the system is tailored to reach a quasi-steady state at this complex frequency—i.e., that after a short transient, the system converges to a response oscillating at the same complex frequency as the input—such excitations can provide an effect analogous to material gain (loss) for $\text{Im}[\omega] < 0$ ($\text{Im}[\omega] > 0$) [21,22]. This principle can support coherent perfect absorption without material loss [19,23], virtual parity-time symmetry without material gain [21], virtual critical coupling [24], negative radiation
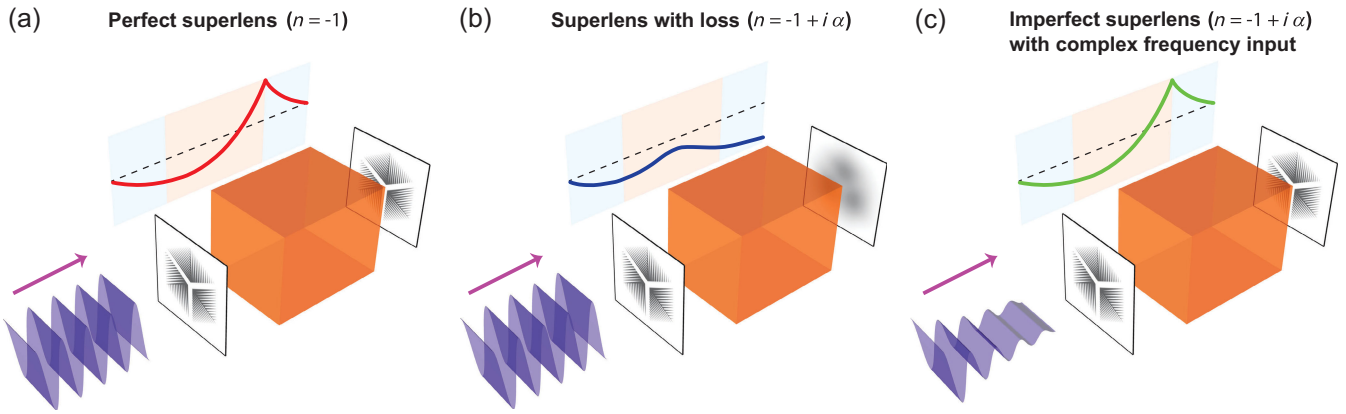
FIG. 1. Superlens response limited by material loss. (a) Superlens without loss, amplifying evanescent fields and providing perfect imaging of an object at the image plane. (b) Material loss in the superlens, which is detrimental to the amplification of evanescent waves, resulting in limited resolution. (c) Excitation at a suitable complex frequency, imparting virtual gain to a passive lossy superlens and enabling an enhancement in resolution and compensation of the detrimental effect of material loss.

pressure [25], and exotic scattering features beyond the limits of passive objects [22].

In this paper, we aim at demonstrating that this concept can be applied to overcome the challenges broadly introduced in the context of metamaterials by material loss. In particular, we focus on the canonical problem of superlensing, one of the prominent applications of metamaterials, which holds the promise of imaging without geometrical aberrations and with deeply subwavelength resolution, with exciting potential for imaging and spectroscopy [26–29]. A planar metamaterial slab with a negative index of refraction, for instance, has been theoretically shown to restore, in its imaging plane, not only propagating waves like a regular lens [30] but also the amplitude of evanescent waves, implying that such a structure can, in principle, achieve enhanced resolution imaging, as sketched in Fig. 1(a) [26]. This intriguing phenomenon is rooted in the exotic wave-matter interactions enabled by negative refractive index materials [30], which can be implemented as metamaterials in various frequency ranges and within several material platforms [31–34]. Despite these exciting prospects, successful implementation of metamaterial superlenses has been limited to date by material loss and nonlocalities, and their application in practical imaging setups has been lagging [35–37]. In particular, larger transverse wave numbers become increasingly more sensitive to material loss [36] and nonlocalities [37], fundamentally limiting the maximum accessible resolution of metamaterial superlenses [36,38]. Figure 1(b) schematizes this concept, showing that evanescent fields can only be partially restored inside an imperfect superlens, limiting the resolution at the image plane.

In the past few years, it has been noticed that it may be possible to go around some of these limitations by controlling the evolution in time of the incident signals. For instance, time-reversal techniques have been used to mimic the growth of the evanescent portion of the spectrum, exceeding the diffraction limit [39,40]. These techniques, however, rely on active systems, which imply a processing delay of the received signals and the need for complex and energy-intensive techniques for time reversal. Transmission matrix and adaptive optics using spatial-light modulators have also enabled imaging beyond the diffraction limit, but the complete characterization of the scattering medium is a prerequisite. Superoscillations have been explored to enhance the imaging resolution by exciting multiple sub-diffraction modes [41,42]. This approach, however, targets specific details of an object, with limitations in the case of complex images. It has also been theoretically shown that, when the monochromatic excitation of a negative-index slab is abruptly shut down [43], the resolution at the image plane can be enhanced. Recent theoretical studies have proposed that pulsed excitations may provide "power" matched evanescent fields after a few periods, enhancing the resolution of metamaterial lenses [44]. Here, we demonstrate that virtual gain, realized through complex frequency excitations, can be used to effectively compensate material loss in metamaterial superlenses, restoring their deeply subwavelength resolution despite the presence of realistic material loss, as schematically shown in Fig. 1(c). Quite importantly, this effect does not lead to instabilities or noise as in the case of material gain, being based on linear, passive, time-invariant systems.

II. POOR-MAN SUPERLENS

In order to shed light on this phenomenon, we start by considering a poor-man superlens formed by a nonmagnetic planar thin slab of thickness $h = 10$ nm with Drude permittivity $\varepsilon(\omega) = \varepsilon_h - (\varepsilon_s - \varepsilon_h)\omega_p^2/(\omega^2 + i\,2\omega\alpha)$, where $\varepsilon_h = 5.45$, $\varepsilon_s = 6.18$, ω_p is the plasma frequency, and $\alpha = 5 \times 10^{14}$ rad/s is the loss rate. In order to study its imaging properties, we consider the transmission from
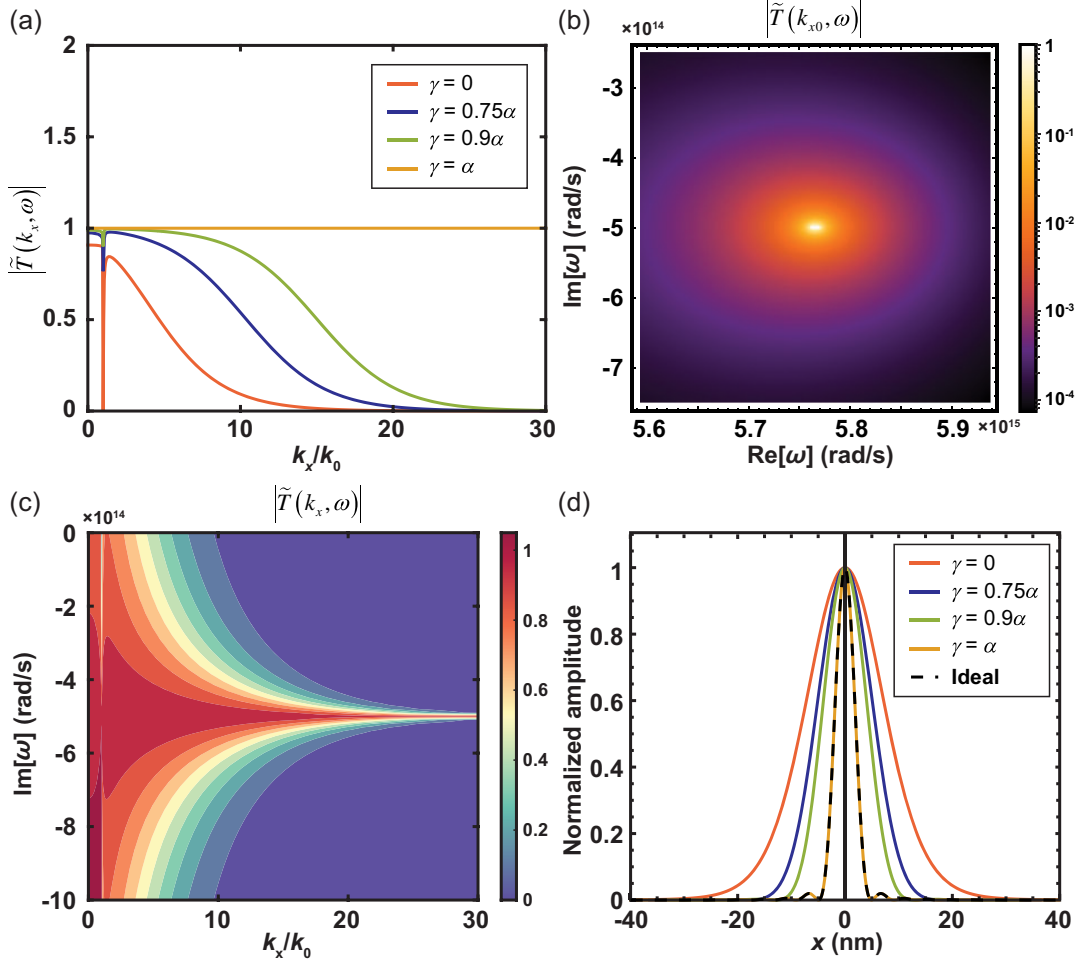
FIG. 2. Virtual gain compensating material absorption in a Drude superlens. (a) Transmission versus transverse wave number for various decay rates $\gamma = 0$ (harmonic), 0.75α, 0.9α, and α. The impinging waves oscillate at the same real part of ω_c with different decay rates. At $\gamma = \alpha$ (yellow curve), the dispersion becomes identical to the dispersion of the ideal. (b) Normalized transmission $|\tilde{T}(k_{x0}, \omega)|$ for $k_{x0} = 30k_0$. The transmission is unitary at complex frequency $\omega_c = 5.77 \times 10^{15} - i\, 5 \times 10^{14}$ rad/s. (c) Density map of the transmission as a function of decay rate and k_x, confirming that transmission is unity when the decay rate is equal to the intrinsic loss rate of the system. (d) Point spread function in the image plane for $\gamma = 0$, 0.75α, 0.9α, and α. As the decay rate approaches the loss rate, the function becomes close to the lossless scenario (dotted curve). The width of the function at $\gamma = \alpha$ is about 5 times smaller than the width of the function at $\gamma = 0$.

object to image plane as a function of the transverse wave number k_x [26],

$$T(k_x, \omega) = \frac{4k_z q_z \varepsilon \exp(iq_z h)}{(q_z + \varepsilon k_z)^2 - (q_z - \varepsilon k_z)^2 \exp(2iq_z h)}, \quad (1)$$

where $q_z = \sqrt{\mu\varepsilon k_0^2 - k_x^2}$ and $k_z = \sqrt{k_0^2 - k_x^2}$ are the wave numbers inside and outside the medium in the longitudinal direction z. In the absence of material loss ($\alpha = 0$), the evanescent waves impinging on the slab with $k_x > k_0$ are amplified in the z direction, resulting in compensation of their decay in air and ensuring that their amplitude is restored on the image plane. In the presence of loss, however, the evanescent fields are less amplified,

consistent with Fig. 1(b) and the red curve in Fig. 2(a), and a cutoff emerges for large wave numbers $k_{\mathrm{cutoff}} = -\ln[|\mathrm{Im}(\varepsilon)/2|^2]/(2h) = 3.1k_0$ [36,38], limiting the device resolution.

Next, we explore an excitation at complex frequency $E_i(t) = E_0 \exp(-i\mathrm{Re}[\omega_c]t) \exp(\mathrm{Im}[\omega_c]t)$, whose negative imaginary part describes an exponentially decaying envelope $\gamma = -\mathrm{Im}[\omega_c]$. Assuming that we can analytically continue Eq. (1), Fig. 2(a) shows the calculated transmission coefficient $\tilde{T}(k_x, \omega) = T(k_x, \omega)/T_{\mathrm{lossless}}$, normalized to the lossless scenario T_{lossless}, for different values of γ. For $\gamma = 0$, the transmission has a cutoff around $k_x \approx 10k_0$ (red curve). However, as we move in the complex frequency plane, the transmission significantly improves,

e.g., $\gamma = 0.75\alpha$ and $\gamma = 0.9\alpha$ for the blue and green curves in Fig. 2(a), respectively. Full recovery of the imaging properties is found when the decay rate γ is equal to the material loss rate α (yellow curve), restoring the ideal resolving features of a lossless superlens [44]. These results are meaningful only under the assumption that the superlens output reaches a quasi-steady state that oscillates at the same complex frequency as the excitation, for which the analytical continuation of Eq. (1) has a physical meaning [22]. Indeed, for $\gamma = 0.75\alpha$, $\gamma = 0.9\alpha$, and $\gamma = \alpha$, the Drude permittivity evaluated at such complex frequency is $\varepsilon = -0.991 + i\,0.277$, $\varepsilon = -0.999 + i\,0.111$, and $\varepsilon = -1$, respectively, compensating for the material loss and explaining why the superlens operation is restored [26]. We may interpret this result as a form of impedance matching enabled by the complex frequency excitation. In the absence of loss, each wave composing the image, independent of its transverse momentum, is impedance matched at the two superlens interfaces for propagating waves [$Z_{\mathrm{lens}}(k_x) = Z_0(k_x)$], while it supports a transverse resonance for evanescent waves [$Z_{\mathrm{lens}}(k_x) = -Z_0(k_x)$]. In the presence of losses, these conditions deviate from the ideal scenario, impacting the field restoration in the imaging plane. Large transverse momenta, associated with subwavelength details of the image, are particularly impacted by this impedance mismatch, even for a small material loss. Operating at a complex frequency restores impedance matching and resonance conditions, explaining the improvement in the superlens performance (see Sec. S1 of Supplemental Material [45] for details).

This result indicates that the detrimental impact of material loss can, in principle, be compensated by a suitably chosen complex frequency excitation. In Fig. 2(b), we show the density plot of normalized transmission in the complex frequency plane for a large transverse wave number $k_{x0} = 30k_0$, finding that the transmission becomes unity for $\omega_c = 5.77 \times 10^{15} - i\,5 \times 10^{14}$ rad/s. Hence, we can expect that, if the slab reaches a quasi-steady state, we may expect a complete restoration of its imaging properties. In this scenario, the material loss is compensated by virtual gain stemming from the excitation. Figure 2(c) shows the transmission density plot as a function of k_x and γ, which becomes unity for all wave numbers when $\gamma = \alpha$. Equivalently, Fig. 2(d) shows the point spread function for the scenarios considered in Fig. 2(a), i.e., the normalized amplitude on the image plane for a delta-function source as we vary the decay rates $\gamma = 0$ (harmonic), $\gamma = 0.75\alpha$, $\gamma = 0.9\alpha$, and $\gamma = a$. The spread functions get narrower as the decay rate approaches the loss rate, and the width of the spread function is minimal for $\gamma = \alpha$,

confirming that the right amount of virtual gain enables complete recovery of the performance of lossy superlenses. Further discussion on a realistic scenario using SiC slabs is given in Sec. 2 of Ref. [45]. While these results are limited to numerical simulations, the prospect of realizing these phenomena in practical imaging devices is indeed realistic. The main challenge arises in making sure that the required decay rate is compatible with conventional modulators and waveform generators that can synthesize the required signals. Operating at lower frequencies, in the radio-frequency and infrared spectra, may simplify the challenge, but for tailored superlenses with sufficiently large quality factors, and hence a reduced value of $\gamma = a$, higher operational frequencies may also be accessible.

III. ACOUSTIC SUPERLENS

In order to demonstrate this phenomenon experimentally, here we consider a holey acoustic metamaterial operating as a superlens for sound. The device features deeply subwavelength periodic square holes and an overall thickness h, as shown in Fig. 3(a). Such a structure has been proposed as an effective acoustic superlens, yielding a resolution well beyond the diffraction limit by relying on acoustic spoof plasmons mediating the transfer of the entire spectrum of an image by transforming the evanescent portion of the impinging spectrum into propagating waves inside the metamaterial and fully transferring it to the image plane through a longitudinal Fabry-Perot (FP) resonance [46]. This type of superlensing device works as an endoscope, avoiding the amplification of evanescent waves but presenting a similar transfer function and hence similar limitations in the presence of material loss. Previous studies have demonstrated how this holey metamaterial indeed operates analogously to a superlens [47,48], albeit operating on scalar acoustic fields [46,49] that suffer from the same resolution limit as optics (see Sec. S3 of Ref. [45] for further details about the comparison between optical and acoustic scenarios). This acoustic superlens forms a powerful platform to evaluate the benefits of virtual gain to enhance the resolution of practical superlenses since it involves a tabletop implementation and operates at lower frequencies, making it easier to control the temporal modulation of the input signal and the evolution of the images at the focal plane. The inset of Fig. 3(a) illustrates the zoomed cross section displaying the square lattice with periodicity d and air-hole size a surrounded by rigid boundaries. The transmission as a function of transverse wave number through such holey structures in the subwavelength regime $\lambda \gg a$, d is given by [49]

$$T_a(k_x, \omega) = \frac{4Y_{\mathrm{hole}}Y_0|S^{(0)}|^2 \exp(iq_{z,a}h)}{(Y_{\mathrm{hole}} + Y_0|S^{(0)}|^2)^2 - (Y_{\mathrm{hole}} - Y_0|S^{(0)}|^2)^2 \exp(2ig_{z,a}h)}, \tag{2}$$
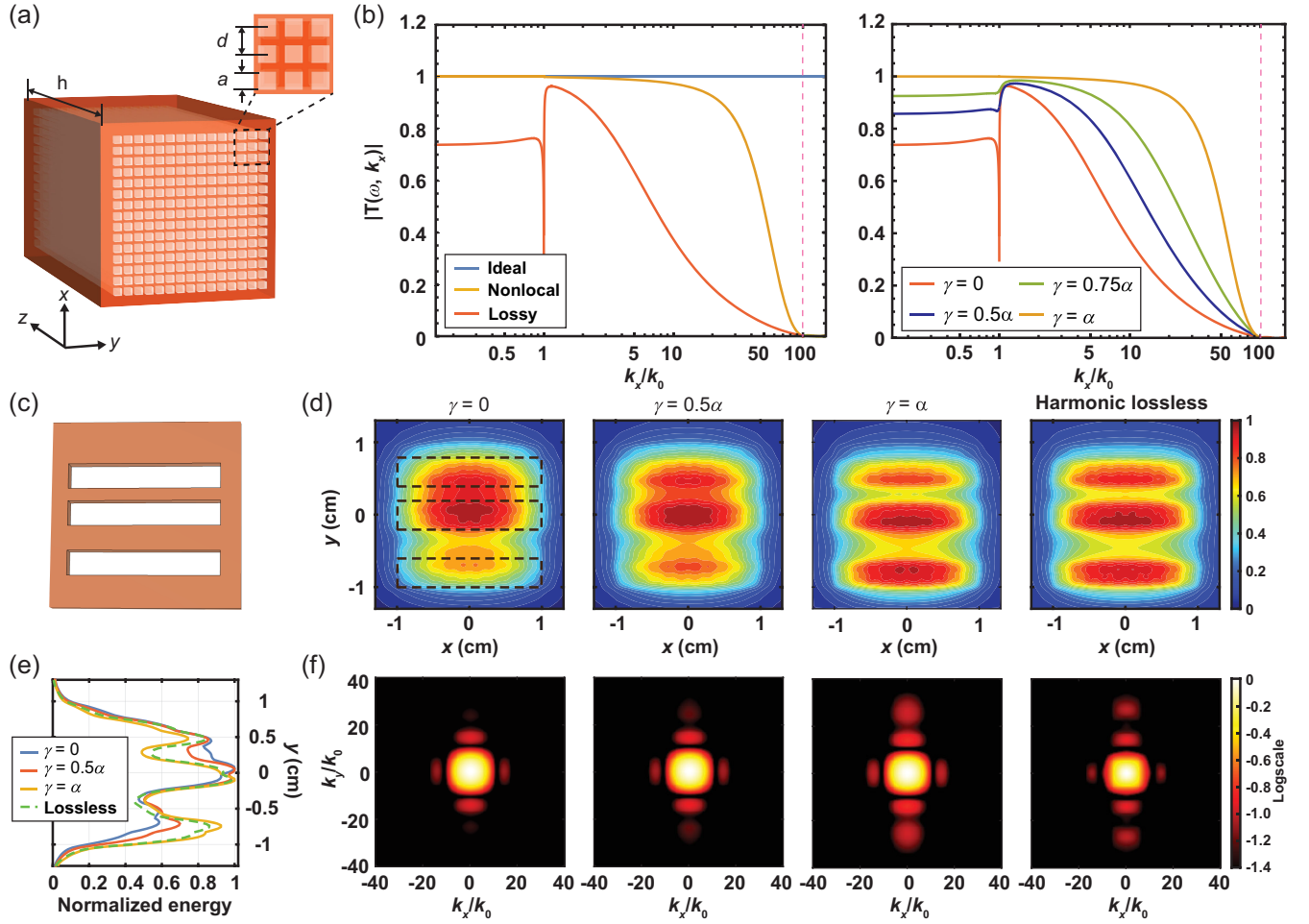
FIG. 3. Holey acoustic metamaterial under complex frequency excitation. (a) Schematic of the acoustic metamaterial with thickness $h = 10$ cm. The size of the square holes is $a = 0.15$ cm, and the lattice constant is $d = 0.2$ cm. (b, left panel) Transmission versus transverse wave number. The transmission at the first FP resonance is not unity for large k_x (yellow) due to nonlocality, such that its response is fundamentally limited by $2\pi/d \approx 100 k_0$ (red dotted line). In the lossy case, the dispersion (red) deviates from the lossless case (yellow). (b, right panel) Incident waves impinging on the structure at the first FP resonant frequency with different complex frequencies. For $\gamma = \alpha$, the dispersion is identical to the dispersion of the lossless scenario (yellow in the left panel). (c) Schematic of the object plate with three lines. The width is 0.4 cm, and the gaps are 0.2 and 0.4 cm. (d) Sound intensities for various decay rates $\gamma = 0$, 0.5α, and α. The dotted boxes represent the original three-line object. The image at $\gamma = \alpha$ becomes consistent with the image in the harmonic lossless case. (e) Image cut of sound intensities for each case. (f) Two-dimensional spatial Fourier components of the sound maps in Fig. 3(d) (log scale).

where Y_0 and Y_{hole} are the admittance of the zeroth diffraction order mode and of the holes, respectively, and $S^{(0)} = \sqrt{a/d} \sin c(k_x a/2)$ is the overlap integral of the fundamental and incident modes (see Sec. S3 of Ref. [45]) [46,49]. The expression in Eq. (2) is analogous to the expression in Eq. (1), with similar features in terms of resolution cutoff. One remarkable difference is that the wave number inside the metamaterial in the z direction is $q_{z,a} = k_0$ for all transverse wave numbers, due to spatial dispersion; hence, this device does not amplify evanescent fields but simply makes them propagative. In order to ensure full transmission of all transverse wave numbers, we rely on a longitudinal Fabry-Perot resonance,

$q_{z,a} = m\pi/h$, where m is an integer, exploiting the fact that all propagating waves travel with the same phase velocity. Figure 3(b) (left) shows the transmission versus normalized transverse wave number k_x/k_0 for the lossless scenario (yellow curve) at the first-order Fabry-Perot resonance for $h = 10$ cm, $a = 0.15$ cm, and $d = 0.2$ cm, in the case of harmonic excitation. We compare the ideal imaging response (blue line), which neglects nonlocal phenomena, with the transmission of the lossless metamaterial (yellow line), with a cutoff determined by the periodicity $k_x \leq 2\pi/d$ (red dotted line), past which Eq. (2) does not apply any longer. In the presence of realistic material loss with absorption rate α, the dispersion decays faster (orange

line), worsening the resolution. On the right panel of Fig. 3(b), we study the response in the complex frequency plane, for different excitation decay rates $\gamma = 0.5\alpha$, $\gamma = 0.75\alpha$, and $\gamma = \alpha$. Indeed, consistent with the previous results, moving to complex frequencies enhances the response and restores the imaging functionality to the ideal lossless scenario in which nonlocality dominates. In particular, for a decay rate equal to the loss rate $\gamma = \alpha$ (yellow), the transmission becomes identical to the lossless scenario, clearly evidencing the potential of virtual gain also in this acoustic platform.

So far, these results have assumed that analytically continuing Eq. (2) yields a physically meaningful output. However, complex frequency signals are not bounded; hence, they necessarily have to start at a given instant in time and, due to their decay and their non-orthogonality, there is no guarantee that the system will converge within a finite transient to an output oscillating at the same complex frequency [22]. Hence, in order to verify our theoretical predictions, we performed full-wave time-domain simulations for a realistic excitation starting at $t = 0$ and studied the temporal evolution of the response. In order to test the imaging features, we test the metamaterial with an object composed of three parallel lines perforated over a thin rectangle solid plate [Fig. 3(c)]. We place this object next to the holey acoustic superlens and excite it with acoustic waves with same carrier frequency $\mathrm{Re}[\omega_c]$, set at 1715 Hz in order to excite the first FP resonance of the slab, and different amplitude modulations to control the imaginary part γ of the excitation frequency. The width of the lines is 0.4 cm, and the interline spacings are 0.4 cm and 0.2 cm. The transmitted acoustic fields are evaluated at the image plane in real time, and we are particularly interested in the quasi-steady-state regime, for which the output response after a transient oscillates at the same complex frequency as the excitation (see Sec. S3 of Ref. [45]) [21,22]. Material loss is introduced in the simulations through thermos-viscous phenomena, which are expected to dominate the material loss mechanism in practical structures. The output sound intensity image under monochromatic excitation [$\gamma = 0$ in Fig. 3(d)] shows a clear limit in resolution, making it impossible to differentiate the strips of the original object (dotted lines). However, as we increase γ, the spatial resolution of the transmitted image is dramatically enhanced. In particular, for $\gamma = \alpha$, the transmitted intensity map is clearly comparable to the image obtained in the case of a lossless system with monochromatic excitation [right panel of Fig. 3(d)], recovering the sub-wavelength spatial features of the object. This is further evidenced by the image cuts at $x = 0$ presented in Fig. 3(e), where the intensity profiles of the lossless and virtual gain scenarios (green dotted and yellow curves, respectively) are compared. By computing the 2D spatial Fourier transform (FT) of the intensity maps in Fig. 3(d), we extract the transverse spatial Fourier components of each image

[Fig. 3(f)]. The FT maps indeed show stronger contributions from the large transverse wave numbers as the decay rate γ approaches the loss rate α, providing clear evidence of the resolution enhancement associated with complex frequency excitation in a realistic setup. Notably, the FT map for $\gamma = \alpha$ is almost identical to the lossless scenario in the right panel of Fig. 3(f). We further analyze these results in Secs. S3 and S4 of Ref. [45]. These simulations confirm that analytical continuation of Eq. (2) is indeed meaningful, and the response of the superlens reaches a quasi-steady state in which virtual gain compensates the detrimental effects of material loss.

We have realized a 3D-printed holey-structured acoustic metamaterial, which expectedly has non-negligible loss due to thermos-viscous dissipation as well as fabrication inaccuracies. We placed the three-line object [left top panel in Fig. 4(a)] on one side of the metamaterial right next to the holes and added a screen sheet on the other side to measure the transmitted pressure fields with a 3D laser vibrometer (see Sec. S4 of Ref. [45] for detailed information on our experiment). The measured, normalized, acoustic energy averaged over one cycle for various complex frequency excitations with $\gamma = 0$, 30, 60, 90, 120, 150, and 180 Hz in the quasi-steady state is shown in Fig. 4(a) (top row). These results are obtained after a short transient, as the acoustic superlens rapidly reaches the quasi-steady state after a few cycles of the excitation. Strikingly, the resolution of the acoustic image drastically improves as virtual gain is added, reaching a maximum for $\gamma = \alpha \approx 180$ Hz. Similar to the simulations, we computed the corresponding spatial FT, whose evolution as a function of the decay is displayed in Fig. 4(a) (bottom row). Focusing on the Fourier components in the y direction, we show the measured transmission normalized to the monochromatic excitation for each transverse wave number in Fig. 4(b). Indeed, virtual gain stemming from complex frequency excitation significantly enhances the transmission of large transverse wave numbers associated with the evanescent spectrum of the image, explaining the observed resolution improvement. For $\gamma = \alpha \approx 180$ Hz, large wave numbers are transmitted with a 6-times enhancement compared to the harmonic excitation case. This effect is further corroborated in the case of more complex 2D objects consisting of the letter E and a smiley face [Fig. 4(c)]. The comparison between the normalized intensities at $\gamma = 0$ (harmonic), $\gamma = \alpha/2$ (90 Hz), and $\gamma = \alpha$ (180 Hz) shows a significant imaging resolution improvement, allowing us to retrieve most of the object's sub-wavelength features.

IV. DISCUSSION

In this work, we have demonstrated that virtual gain obtained by precisely tailoring incident signals oscillating at complex frequencies can be used to compensate for the adverse effects of material loss in passive superlenses. We
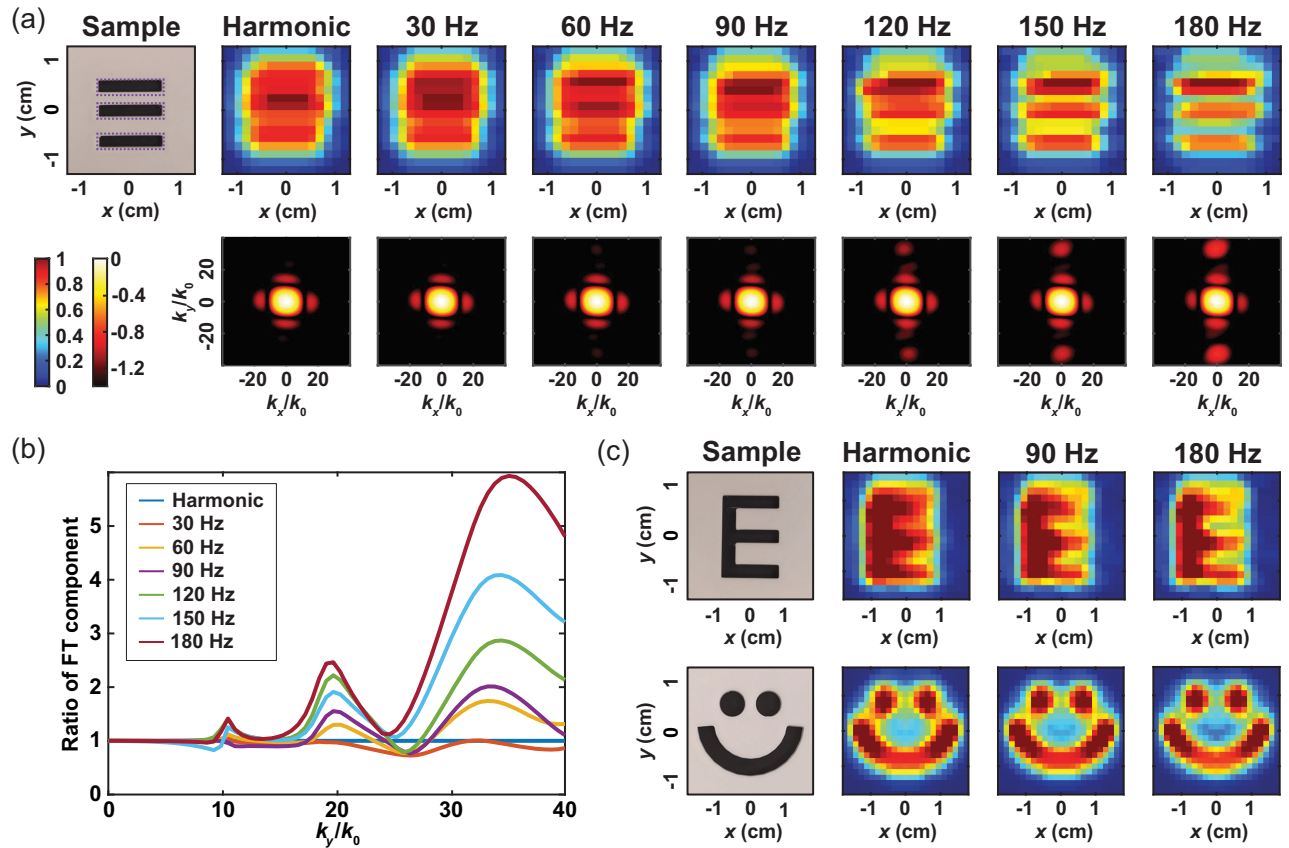
FIG. 4. Experimental demonstration of virtual acoustic superlens. (a) Three-line object, sound maps in real and reciprocal spaces for each case. The maps represent acoustic energy normalized by each maximum. Once the decay rate is close to the loss rate $\alpha \approx 180$ Hz, the image map is optimally resolved. (b) One-dimensional Fourier components for different decay rates normalized to the same transverse wave number in the harmonic excitation case. (c) Comparison of letter E (top) and smiley face (bottom) images under harmonic and complex frequency excitations. Here, the decay rates of the complex excitation are 90 and 180 Hz.

theoretically and numerically validated the concept in optics for the case of a poor-man superlens and experimentally implemented virtual gain-assisted loss compensation in a holey acoustic metamaterial superlens, verifying that, when the decay rate of the impinging excitation matches the intrinsic loss rate of the superlens, a restoration of the subwavelength features of the image is achievable, implementing a much-improved superlens whose resolution is limited only by nonlocalities. Importantly, complex frequency excitations have a finite frequency bandwidth, which should be considered for the definition of the diffraction limit. Nevertheless, the requirement that the superlens reaches a quasi-steady state, which is necessary to be able to observe this phenomenon, implies that the structures support a high quality factor, and as such, the finite bandwidth of the excitation is narrow. Hence, the actual frequencies exciting the structure are still concentrated within a limited range around the central frequency, and our results clearly demonstrate deeply subwavelength imaging. Indeed, the demonstrated resolution enhancement is directly related to the virtual gain phenomenon, as further discussed in Sec. S6 of Ref. [45].

Our approach to compensate loss and enhance the resolution of imaging devices does not require active elements, signal processing, or feedback, and since the structure necessarily supports a large quality factor, it operates for a relatively long temporal range within the quasi-stationary regime, opening numerous opportunities for imaging, which may go beyond acoustics and be extended to nano-optics [28,29]. While translating this technique to optical superlenses may be challenging due to the much faster temporal evolution of the input signals in the visible wavelength spectrum, an alternative approach involves synthesizing the temporal waveform using multiple monochromic excitations, as recently proposed in Ref. [50]. However, image postprocessing is required in this approach. Quite remarkably, recent studies have demonstrated that complex frequency excitations and virtual gain can be realized in silicon nitride photonic circuits with a high Q factor ($Q \sim 10^4$) operating at a wavelength of 1550 nm, demonstrating the feasibility of this approach in the optical regime [51]. More broadly, our results pave the way for loss compensation in a variety of metamaterial, photonic, and acoustic platforms, offering a

plethora of opportunities for imaging, sensing, lithography, computing, and communications, and may also be extended to quantum technologies.

[1] L. D. Landau, J. S. Bell, M. Kearsley, L. Pitaevskii, E. Lifshitz, and J. Sykes, *Electrodynamics of Continuous Media* (Elsevier, New York, 2013), Vol. 8.

[2] J. B. Khurgin, *How to Deal with the Loss in Plasmonics and Metamaterials*, Nat. Nanotechnol. **10**, 2 (2015).

[3] J. Elser, V. A. Podolskiy, I. Salakhutdinov, and I. Avrutsky, *Nonlocal Effects in Effective-Medium Response of Nano-layered Metamaterials*, Appl. Phys. Lett. **90**, 191109 (2007).

[4] D. Ö. Güney, T. Koschny, and C. M. Soukoulis, *Reducing Ohmic Losses in Metamaterials by Geometric Tailoring*, Phys. Rev. B **80**, 125129 (2009).

[5] A. Boltasseva and H. A. Atwater, *Low-Loss Plasmonic Metamaterials*, Science **331**, 290 (2011).

[6] S. A. Ramakrishna, J. B. Pendry, M. C. K. Wiltshire, and W. J. Stewart, *Imaging the Near Field*, J. Mod. Opt. **50**, 1419 (2003).

[7] D. R. Smith and D. Schurig, *Electromagnetic Wave Propagation in Media with Indefinite Permittivity and Permeability Tensors*, Phys. Rev. Lett. **90**, 077405 (2003).

[8] S. Anantha Ramakrishna and J. B. Pendry, *Removal of Absorption and Increase in Resolution in a Near-Field Lens Via Optical Gain*, Phys. Rev. B **67**, 201101(R) (2003).

[9] S. Wuestner, A. Pusch, K. L. Tsakmakidis, J. M. Hamm, and O. Hess, *Overcoming Losses with Gain in a Negative Refractive Index Metamaterial*, Phys. Rev. Lett. **105**, 127401 (2010).

[10] S. Xiao, V. P. Drachev, A. V. Kildishev, X. Ni, U. K. Chettiar, H.-K. Yuan, and V. M. Shalaev, *Loss-Free and Active Optical Negative-Index Metamaterials*, Nature (London) **466**, 735 (2010).

[11] A. Ghoshroy, Ş. K. Özdemir, and D. Ö. Güney, *Loss Compensation in Metamaterials and Plasmonics with Virtual Gain [Invited]*, Opt. Mater. Express **10**, 1862 (2020).

[12] A. Krasnok and A. Alù, *Active Nanophotonics*, Proc. IEEE **108**, 628 (2020).

[13] W. Adams, A. Ghoshroy, and D. Ö. Güney, *Incoherent Active Convolved Illumination Enhances the Signal-to-Noise Ratio for Shot Noise: Experimental Evidence*, Phys. Rev. Appl. **18**, 064080 (2022).

[14] P. Kinsler and M. W. McCall, *Causality-Based Criteria for a Negative Refractive Index Must Be Used with Care*, Phys. Rev. Lett. **101**, 167401 (2008).

[15] M. P. H. Andresen, A. V. Skaldebø, M. W. Haakestad, H. E. Krogstad, and J. Skaar, *Effect of Gain Saturation in a Gain Compensated Perfect Lens*, J. Opt. Soc. Am. B **27**, 1610 (2010).

[16] M. I. Stockman, *Nanoplasmonics: Past, Present, and Glimpse into Future*, Opt. Express **19**, 22029 (2011).

[17] P. A. Sturrock, *Kinematics of Growing Waves*, Phys. Rev. **112**, 1488 (1958).

[18] B. Nistad and J. Skaar, *Causality and Electromagnetic Properties of Active Media*, Phys. Rev. E **78**, 036603 (2008).

[19] D. G. Baranov, A. Krasnok, and A. Alù, *Coherent Virtual Absorption Based on Complex Zero Excitation for Ideal Light Capturing*, Optica **4**, 1457 (2017).

[20] A. Krasnok, D. Baranov, H. Li, M.-A. Miri, F. Monticone, and A. Alú, *Anomalies in Light Scattering*, Adv. Opt. Photonics **11**, 892 (2019).

[21] H. Li, A. Mekawy, A. Krasnok, and A. Alù, *Virtual Parity-Time Symmetry*, Phys. Rev. Lett. **124**, 193901 (2020).

[22] S. Kim, S. Lepeshov, A. Krasnok, and A. Alù, *Beyond Bounds on Light Scattering with Complex Frequency Excitations*, Phys. Rev. Lett. **129**, 203601 (2022).

[23] G. Trainiti, Y. Ra'di, M. Ruzzene, and A. Alù, *Coherent Virtual Absorption of Elastodynamic Waves*, Sci. Adv. **5**, eaaw3255 (2019).

[24] Y. Ra'di, A. Krasnok, and A. Alù, *Virtual Critical Coupling*, ACS Photonics **7**, 1468 (2020).

[25] S. Lepeshov and A. Krasnok, *Virtual Optical Pulling Force*, Optica **7**, 1024 (2020).

[26] J. B. Pendry, *Negative Refraction Makes a Perfect Lens*, Phys. Rev. Lett. **85**, 3966 (2000).

[27] R. A. Shelby, D. R. Smith, and S. Schultz, *Experimental Verification of a Negative Index of Refraction*, Science **292**, 77 (2001).

[28] N. Fang, H. Lee, C. Sun, and X. Zhang, *Sub-Diffraction-Limited Optical Imaging with a Silver Superlens*, Science **308**, 534 (2005).

[29] T. Taubner, D. Korobkin, Y. Urzhumov, G. Shvets, and R. Hillenbrand, *Near-Field Microscopy through a SiC Superlens*, Science **313**, 1595 (2006).

[30] V. G. Veselago, *The Electrodynamics of Substances with Simultaneously Negative Values of ε and μ*, Sov. Phys. Usp. **10**, 509 (1968).

[31] G. V. Eleftheriades, O. Siddiqui, and A. K. Iyer, *Transmission Line Models for Negative Refractive Index Media and Associated Implementations without Excess Resonators*, IEEE Microw. Wirel. Compon. Lett. **13**, 51 (2003).

[32] D. R. Smith, J. B. Pendry, and M. C. K. Wiltshire, *Metamaterials and Negative Refractive Index*, Science **305**, 788 (2004).

[33] N. Engheta and R. W. Ziolkowski, *Metamaterials: Physics and Engineering Explorations* (John Wiley & Sons, New York, 2006).

[34] N. Kaina, F. Lemoult, M. Fink, and G. Lerosey, *Negative Refractive Index and Acoustic Superlens from Multiple Scattering in Single Negative Metamaterials*, Nature (London) **525**, 77 (2015).

[35] C. Luo, S. G. Johnson, J. D. Joannopoulos, and J. B. Pendry, *All-Angle Negative Refraction without Negative Effective Index*, Phys. Rev. B **65**, 201104(R) (2002).

[36] V. A. Podolskiy and E. E. Narimanov, *Near-Sighted Superlens*, Opt. Lett. **30**, 75 (2005).

[37] X.-X. Liu and A. Alu, *Limitations and Potentials of Metamaterial Lenses*, J. Nanophoton. **5**, 053509 (2011).

[38] D. R. Smith, D. Schurig, M. Rosenbluth, S. Schultz, S. A. Ramakrishna, and J. B. Pendry, *Limitations on Sub-diffraction Imaging with a Negative Refractive Index Slab*, Appl. Phys. Lett. **82**, 1506 (2003).

[39] G. Lerosey, J. de Rosny, A. Tourin, and M. Fink, *Focusing Beyond the Diffraction Limit with Far-Field Time Reversal*, Science **315**, 1120 (2007).

[40] A. P. Mosk, A. Lagendijk, G. Lerosey, and M. Fink, *Controlling Waves in Space and Time for Imaging and Focusing in Complex Media*, Nat. Photonics **6**, 283 (2012).

[41] M. Dubois, E. Bossy, S. Enoch, S. Guenneau, G. Lerosey, and P. Sebbah, *Time-Driven Superoscillations with Negative Refraction*, Phys. Rev. Lett. **114**, 013902 (2015).

[42] Y. Eliezer, L. Hareli, L. Lobachinsky, S. Froim, and A. Bahabad, *Breaking the Temporal Resolution Limit by Super-oscillating Optical Beats*, Phys. Rev. Lett. **119**, 043903 (2017).

[43] A. Archambault, M. Besbes, and J.-J. Greffet, *Superlens in the Time Domain*, Phys. Rev. Lett. **109**, 097405 (2012).

[44] A. Rogov and E. Narimanov, *Space–Time Metamaterials*, ACS Photonics **5**, 2868 (2018).

[45] See Supplemental Material at http://link.aps.org/supplemental/10.1103/PhysRevX.13.041024 for the operation of conventional superlenses, provides the temporal analysis of optical and acoustic superlenses, and the description of the numerical methods. We also provide details on the experiments and on the diffraction limit.

[46] J. Zhu, J. Christensen, J. Jung, L. Martin-Moreno, X. Yin, L. Fok, X. Zhang, and F. J. Garcia-Vidal, *A Holey-Structured Metamaterial for Acoustic Deep-Subwavelength Imaging*, Nat. Phys. **7**, 52 (2011).

[47] J. Jung, F. J. García-Vidal, L. Martín-Moreno, and J. B. Pendry, *Holey Metal Films Make Perfect Endoscopes*, Phys. Rev. B **79**, 153407 (2009).

[48] J. B. Pendry, L. Martín-Moreno, and F. J. Garcia-Vidal, *Mimicking Surface Plasmons with Structured Surfaces*, Science **305**, 847 (2004).

[49] J. Christensen, L. Martin-Moreno, and F. J. Garcia-Vidal, *Theory of Resonant Acoustic Transmission through Sub-wavelength Apertures*, Phys. Rev. Lett. **101**, 014301 (2008).

[50] F. Guan, X. Guo, K. Zeng, S. Zhang, Z. Nie, S. Ma, Q. Dai, J. Pendry, X. Zhang, and S. Zhang, *Overcoming Losses in Superlenses with Synthetic Waves of Complex Frequency*, Science **381**, 766 (2023).

[51] J. Hinney, S. Kim, G. J. K. Flatt, I. Datta, A. Alù, and M. Lipson, in *CLEO 2023* (Optica Publishing Group, San Jose, CA, 2023), p. JTh2A.69.